Magn Reson Med Sci 2020; 19; 21–28
doi:10.2463/mrms.mp.2018-0174
Published Online: March 18, 2019

MAJOR PAPER

Pseudo-random Trajectory Scanning Suppresses Motion Artifacts on Gadoxetic Acid-enhanced Hepatobiliary-phase Magnetic Resonance Images

Yuko Nakamura[1*], Toru Higaki[1], Takashi Nishihara[2], Kuniaki Harada[2], Masahiro Takizawa[2], Yoshitaka Bito[2], Keigo Narita[1], Motonori Akagi[1], Yoshiko Matsubara[1], Shogo Kamioka[3], Yuji Akiyama[3], Makoto Iida[1], and Kazuo Awai[1]

Purpose: Hepatobiliary-phase (HBP) MRI with gadoxetic acid facilitates the differentiation between lesions with and without functional hepatocytes. Thus, high-quality HBP images are required for the detection and evaluation of hepatic lesions. However, the long scan time may increase artifacts due to intestinal peristalsis, resulting in the loss of diagnostic information. Pseudo-random acquisition order disperses artifacts into the background. The aim of this study was to investigate the clinical applicability of pseudo-random trajectory scanning for the suppression of motion artifacts on T_1-weighted images including HBP.

Methods: Our investigation included computer simulation, phantom experiments, and a clinical study. For computer simulation and phantom experiments a region of interest (ROI) was placed on the area with motion artifact and the standard deviation inside the ROI was measured as image noise. For clinical study we subjected 62 patients to gadoxetic acid-enhanced hepatobiliary-phase imaging with a circular- and a pseudo-random trajectory (c-HBP and p-HBP); two radiologists graded the motion artifacts, sharpness of the liver edge, visibility of intrahepatic vessels, and overall image quality using a five-point scale where 1 = unacceptable and 5 = excellent. Differences in the qualitative scores were determined using the two-sided Wilcoxon signed-rank test.

Results: The image noise was higher on the circular image compared with pseudo-random image (101.0 vs 60.9 on computer simulation image, 91.2 vs 67.7 on axial, 95.5 vs 86.9 on reformatted sagittal image for phantom experiments). For clinical study the score for motion artifacts was significantly higher with p-HBP than c-HBP imaging (left lobe: mean 3.4 vs 3.2, $P < 0.01$; right lobe: mean 3.6 vs 3.4, $P < 0.01$) as was the qualitative score for the overall image quality (mean 3.6 vs 3.3, $P < 0.01$).

Conclusion: At gadoxetic acid-enhanced hepatobiliary-phase imaging, p-HBP scanning suppressed motion artifacts and yielded better image quality than c-HBP scanning.

Keywords: *hepatobiliary phase, intestinal peristalsis, motion artifacts, pseudo-random trajectory*

Introduction

As hepatobiliary-phase (HBP) MRI with gadoxetic acid yields excellent contrast resolution for the liver parenchyma, it facilitates the differentiation between lesions with and without functional hepatocytes.[1] Thus, high-quality HBP images are required for the detection and evaluation of hepatic lesions.[2–4] However, on abdominal MRI scans, artifacts due to physiologic motion such as respiratory motion, cardiovascular pulsation, bowel movement, and the movement of subjects impair the image quality and lead to loss of diagnostic information. While the integration of a respiratory navigator-gating technique may address problems attributable to respiratory motion,[5–7] the acquisition time is longer and artifacts due to intestinal peristalsis may increase because peristaltic artifacts may occur on abdominal MRI scans even with breath-hold scanning.[8]

Lin et al.[9] introduced a novel method, magnetization-prepared elliptical centric fast gradient echo imaging. It is

[1]Diagnostic Radiology, Hiroshima University, 1-2-3 Kasumi, Minami-ku, Hiroshima, Hiroshima 734-8551, Japan
[2]Healthcare Business Unit, Hitachi, Ltd., Tokyo, Japan
[3]Department of Radiology, Hiroshima University Hospital, Hiroshima, Japan
[*]Corresponding author, Phone: +81-82-257-5257, Fax: +81-82-257-5259, E-mail: yukon@hiroshima-u.ac.jp

Received: December 14, 2018 | Accepted: February 6, 2019

based on recessed elliptical centric view-ordering. The view order is modified so that the data acquisition begins at the outer *k*-space, jumps through the central *k*-space in a pseudo-random fashion, and then returns to the outer *k*-space. They reported that this pseudo-random acquisition order disperses artifacts into the background with little impact on the image quality of brain MRI scans. We hypothesized that pseudo-random acquisition can be used to suppress motion artifacts due to intestinal peristalsis on abdominal MRI scans.

We developed a navigator-gated scanning technique that applies a pseudo-random trajectory to T_1-weighted imaging including HBP for suppression of motion artifact. The purpose of this study was to investigate the clinical applicability of HBP scans obtained with our pseudo-random technique, especially on intestinal peristalsis motion artifact.

Materials and Methods

Our investigation included computer simulation, phantom experiments, and a clinical study.

Pseudo-random trajectory scans

A schema of conventional scanning using a circular trajectory in the $k_y - k_z$ plane is shown in Fig. 1a. Circular-trajectory scanning consists of 101, 470, and 174 shots for computer simulation, phantom experiments, and clinical study, respectively; each shot is comprised of 48, 48, and 80 segments for computer simulation, phantom experiments, and clinical study, respectively scanned continuously (each segment corresponds to each phase encoding step, and the number of shot and segment is fixed); the first half of the segments is scanned radially from the center to the edge, and the second half is scanned circularly and continuously in the $k_y - k_z$ plane. Pseudo-random scanning consists of 101, 470, and 174 shots for computer simulation, phantom experiments, and clinical study, respectively; each shot is comprised of 48, 48, and 80 segments for computer simulation, phantom experiments, and clinical study, respectively same to circular trajectory (the number of shot and segment is fixed). At pseudo-random scanning, the first half of the segments is scanned radially from the center to edge in the same manner as circular trajectory but the second half of the segments is scanned circularly by skipping golden-angle (GA; set as 137.507764 degree), resulting in the pseudo-random sampling (Fig. 1b).[10]

Computer simulation and phantom experiments

Computer simulation

To evaluate motion artifacts due to intestinal peristalsis, two pairs of computer-simulated data roughly mimicking the human abdominal anatomy were created (Fig. 2). Only the position of the intestines differed to simulate motion artifacts due to intestinal peristalsis (Fig. 2-0). To create the simulated image with motion artifacts, we calculated two *k*-space data from the original simulated images on which the position of the intestines differed (Fig. 2-1), separated the *k*-space data into data-subsets from shots 1–25 and 26–101 because this separation induces the artifact for both slice and phase

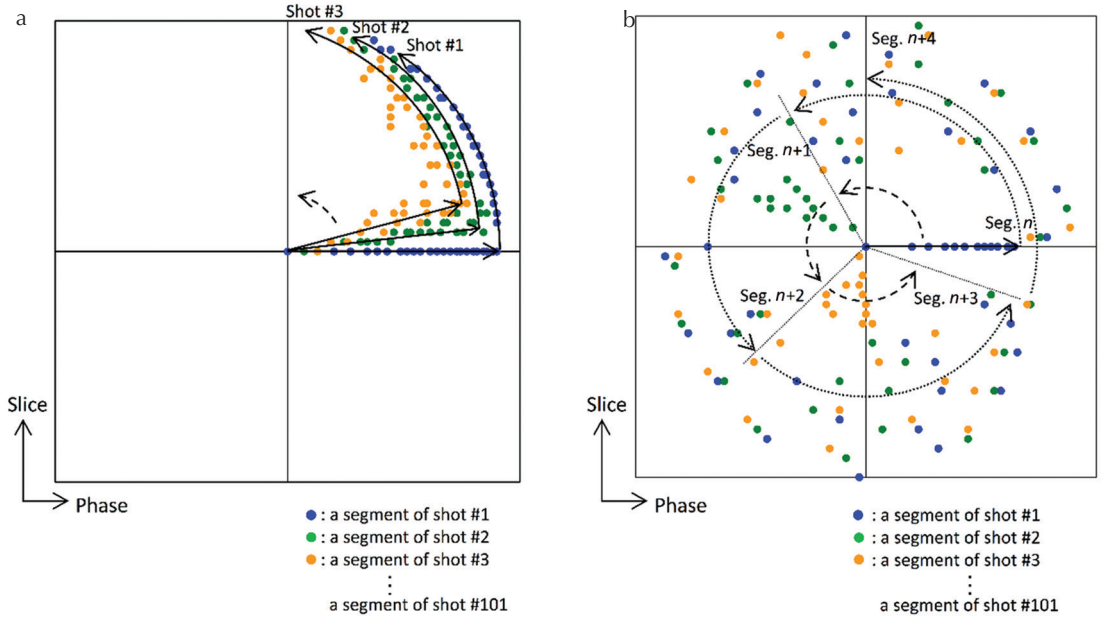

Fig. 1 *k*-Space trajectories of circular- (**a**) and pseudo-random (**b**) scanning. (**a**) The trajectories include 101 shots; each shot consists of 48 segments (dots). The solid lines indicate the *k*-space trajectory of each shot. Segments in each shot were acquired radially and circularly in continuous order. Data from the 101 shots fill the *k*-space along the dashed line. (**b**) During pseudo-random trajectory scanning, the first half of the segments was scanned radially from the center to the edge similarly to the circular trajectory (solid line). The second half was scanned circularly, skipping the golden angle (dotted line), resulting in pseudo-random sampling. Data from the 101 shots data also fill the *k*-space by skipping the golden-angle (dashed line).

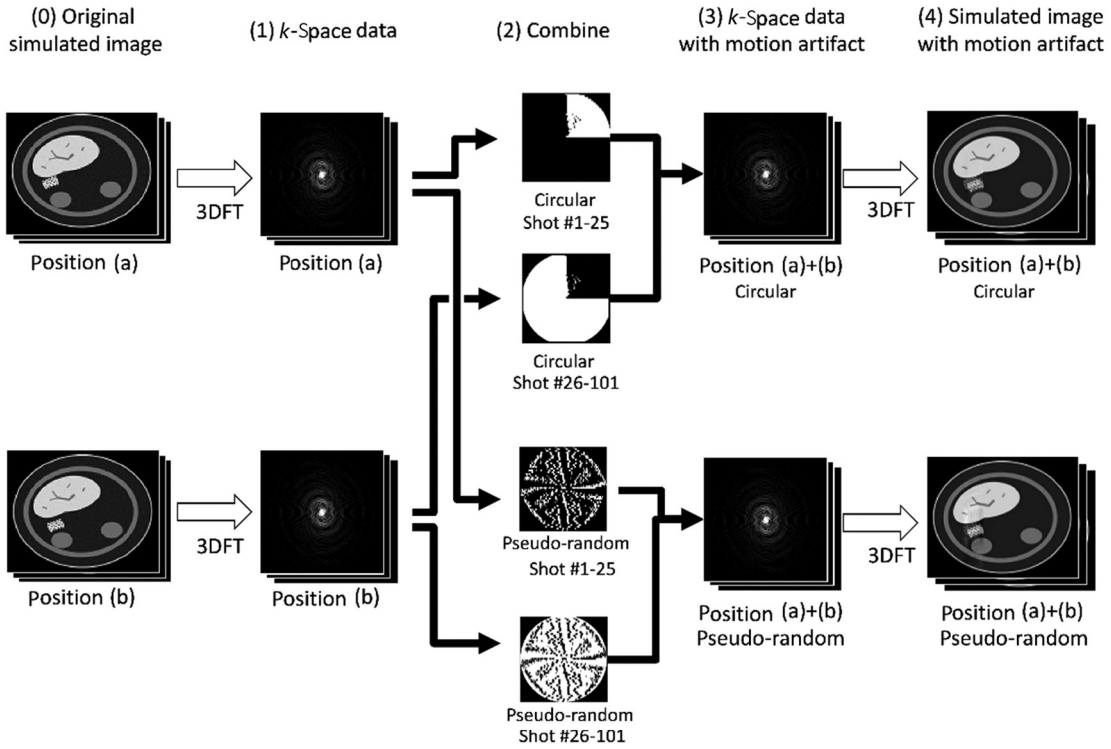

Fig. 2 Schematic diagram of simulated motion artifacts. Motion occurs between shots #25 and #26.

direction and then combined the *k*-space data from position (a; shots 1–25) and position (b; shots 26–101) for each trajectory (Figs. 2-2 and 2-3), and applied 3D Fourier transform to the two *k*-space data with motion artifacts to obtain two simulated image data (Fig. 2-4). Parameters for simulated images were matrix 128 × 128, and the number of slices 48.

Phantom image acquisition

A large and two small bottle phantoms filled with a $NiCl_2$ solution were scanned with a 3T MRI instrument (Hitachi, Ltd., Tokyo, Japan) equipped with 12-channel phased-array receiver coil. To simulate motion artifacts due to intestinal peristalsis, one small bottle was rotated at 3 cm/s during the scan (Fig. 3). A non-gated fat-suppressed 3D T_1-weighted gradient echo nature of the sequence (TIGRE) with parallel imaging (rapid acquisition through a parallel imaging design [RAPID, Hitachi, Ltd., Tokyo, Japan]) was performed applying each trajectory, circular and pseudo-random. Parameters for TIGRE were thickness and interval 1.2 mm, slab thickness 216 mm, TR/TE 4.2/1.8 ms, flip angle (FA) 20°, field of view (FOV) 35 × 28 cm^2, matrix 400 × 320, and parallel imaging factor 1.9 (1.8 for phase direction and 1.1 for slice direction).

Image analysis for computer simulation and phantom experiments

Images were analyzed using ImageJ software (National Institutes of Health, Bethesda, MD, USA, http://rsb.info.nih.gov/ij/). Quantitative analysis was performed by one radiologist (KN with 4 years of experience in radiology). A region of interest (ROI) was placed on the area with motion artifact (Figs. 3 and 4). The mean signal intensity and standard deviation (SD) inside the ROI was measured; the SD value represented the image noise.

Clinical study

This retrospective study was approved by our Institutional Review Board; prior to informed patient consent was waived because it was observational. Patient records and information were anonymized and de-identified prior to analysis.

Study population

We estimated that 57 subjects were the sample size needed to detect a difference between HBP images with a circular- and pseudo-random trajectory (c-HBP and p-HBP); the effect size was 0.5, α was 0.05, and statistical power was 0.95.

Included were 62 consecutive patients who underwent gadoxetic acid-enhanced MRI studies at our institution between March and April 2018. They were 48 males and 14 females; their age ranged from 15 to 88 years (median 65.5 years). Of these, 31 patients were followed up after malignant liver tumor surgery, 16 patients underwent MRI to assess liver lesions detected on ultrasound- or dynamic-CT studies, five patients were followed for benign liver tumors, one patient required staging of a suspected malignant liver tumor, and nine patients were screened for liver tumors.

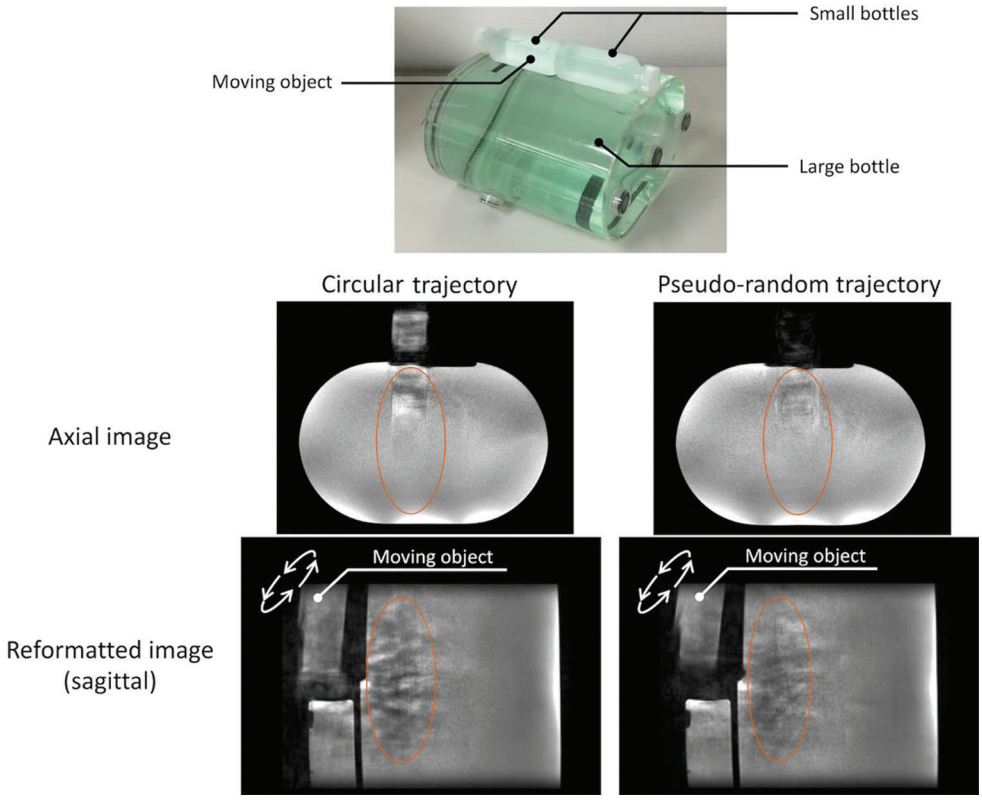

Fig. 3 Real phantom photo and MR images of circular- and pseudo-random trajectory scanning. Motion artifacts are suppressed in the image scanned with pseudo-random trajectory. The image noise (standard deviation [SD] of the circular ROI) is lower in the image scanned with pseudo-random trajectory.

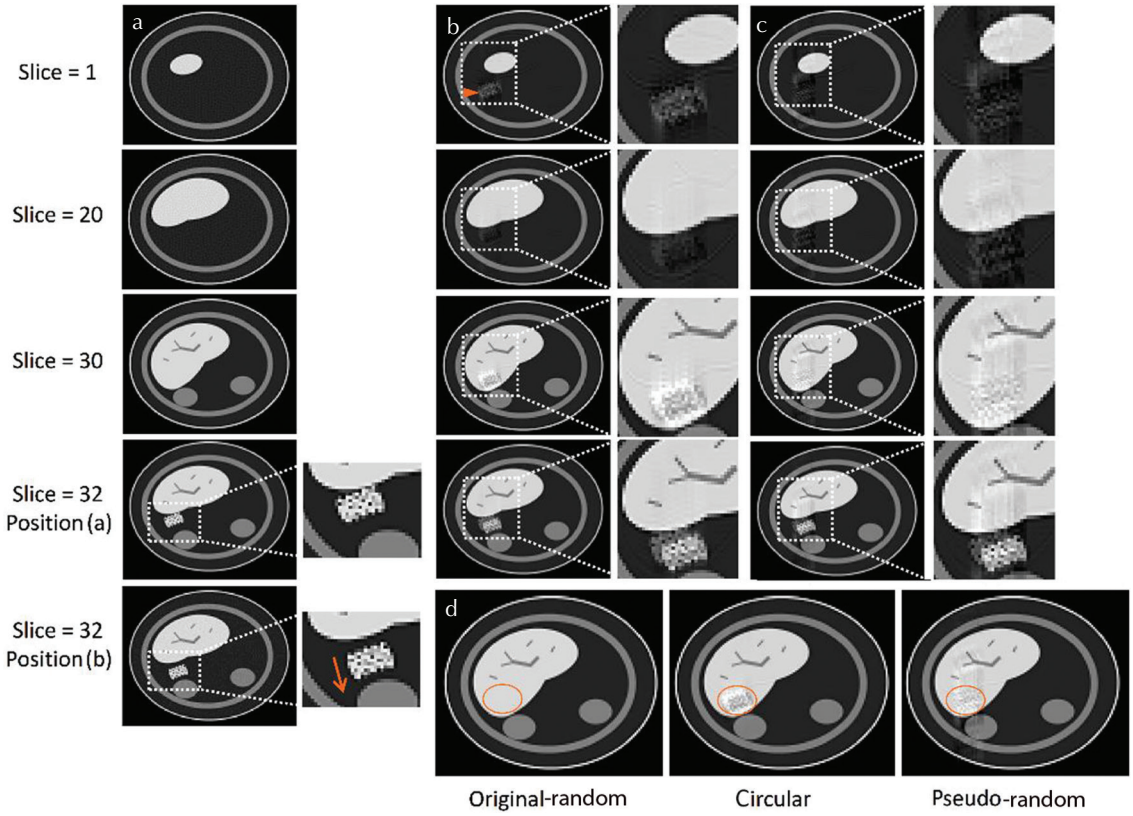

Fig. 4 Simulation of motion artifacts. Original- (**a**), circular- (**b**) and pseudo-random trajectory image (**c**). Pseudo-random trajectory scanning disperses the motion artifacts. The image noise (standard deviation [SD] of the circular ROI) is lower on the pseudo-random than the circular trajectory image (**d**).

Two patients had undergone right hepatectomy and four left hepatectomy.

Image acquisition

Magnetic contrast enhancement was obtained by the intravenous administration of 25 μmol/kg of gadoxetic acid (EOB-Primovist, Bayer Yakuhin, Osaka, Japan) injected at a rate of 2.0 ml/s followed by 20 ml of saline delivered at the same rate using a power injector (Sonic Shot 50; Nemoto-Kyorindo, Tokyo, Japan).

Circular- and pseudo-random-hepatobiliary-phase imaging was initiated 20 min after the gadoxetic-acid injection. HBP imaging was with TIGRE with parallel imaging (RAPID) using navigator echo-based respiratory gating technique (section thickness and interval 1.8 mm, slab thickness 216 mm, TR/TE 4.0 ms/1.8 ms, FA 15°, FOV 36 × 27 cm^2, matrix 332 × 216, parallel imaging factor 3 [2.0 for phase direction and 1.5 for slice direction]). The scanner was the same 3T MRI instrument used in the phantom study. All images were obtained in the transverse plane. Although dynamic MRI scans using gadoxetic acid were obtained for the clinical studies they were not evaluated in this study.

Image analysis

The image quality was independently evaluated by two board-certified radiologists (YN and KA with 14 and 31 years of experience in radiology). Images were presented in random order; the recorded scores were reached by consensus. Both readers were given standardized instructions and were trained on image sets from five patients who were not included in this study. They ranked motion artifacts, sharpness of the liver edge, visibility of intrahepatic vessels (evaluating the conspicuity of portal and hepatic vein of whole liver), and overall image quality based on a previously reported grading system (Likert Scale). Qualitative scores were recorded on a five-point scale. For motion artifacts:1 = extensive artifacts, non-diagnostic; 2 = severe artifacts, image degraded but interpretable; 3 = moderate artifacts, some effect on diagnostic quality; 4 = minimal artifacts, no effect on diagnostic quality; 5 = no motion artifact. For sharpness of the liver edge: 1 = non-identifiable, non-diagnostic; 2 = obscure, image degraded but interpretable; 3 = moderately blurred, some effect on diagnostic quality; 4 = almost clear, no effect on diagnostic quality; 5 = clearly visible. For visibility of intrahepatic vessels: 1 = non-identifiable, non-diagnostic; 2 = obscure, image degraded but interpretable; 3 = moderately blurred, some effect on diagnostic quality; 4 = almost clear, no effect on diagnostic quality; 5 = clearly visible. For overall image quality: 1 = unacceptable, 2 = suboptimal, 3 = acceptable, 4 = good, 5 = excellent.[11–13]

Statistical analysis

Statistically significant differences were evaluated with JMP 10 software (SAS Institute, Cary, NC, USA). Differences in the qualitative scores were determined using the two-sided Wilcoxon signed-rank test. Differences of $P < 0.05$ were considered statistically significant.

For qualitative analysis, we calculated interobserver agreement using the weighted kappa statistic. A kappa statistic in the range of 0.81–1.00 was interpreted as excellent, 0.61–0.80 as substantial, 0.41–0.60 as moderate, 0.21–0.40 as fair, and 0–0.20 as poor agreement.[14]

Results

Computer simulation study

On circular trajectory images, we observed high signal intensity due to motion artifacts on the posterior side of the liver (Fig. 4b). On pseudo-random images, high signal intensity due to motion artifacts was dispersed into the slice and phase direction. This resulted in an image noise reduction especially on the posterior side of the liver (Fig. 4c). The mean signal intensity inside the ROI was 651.0, 629.8, and 650.2 on the original-, the circular-, and the pseudo-random image, respectively. The image noise was 0.0, 101.0, and 60.9 on the original-, circular-, and pseudo-random image, respectively (Fig. 4d).

Phantom study

As in the computer simulation study, motion artifacts were lower on pseudo-random than circular images (Figs. 3a and 3b). The mean signal intensity inside the ROI was 709.0 and 701.4 for axial circular- and pseudo-random images, and 694.6 and 684.9 for reformatted sagittal circular- and pseudo-random images, respectively. The image noise was 91.2 and 67.7 for axial circular- and pseudo-random images, and 95.5 and 86.9 for sagittal circular- and pseudo-random images, respectively.

Clinical study

Scanning time for each trajectory was around 3 min; scanning time was almost equivalent between two trajectories.

As shown in Table 1, the scores for motion artifacts were significantly better for p-HBP than c-HBP images (left lobe: mean 3.4 vs 3.2, right lobe: 3.6 vs 3.4; all, $P < 0.01$) (Figs. 5 and 6). There was no significant difference in the score for

Table 1 Subjective image quality scores for motion artifacts

	Left lobe		Right lobe	
	c-HBP	p-HBP	c-HBP	p-HBP
Score 1	0	0	0	0
Score 2	13	10	8	6
Score 3	24	21	27	21
Score 4	20	21	21	25
Score 5	1	6	5	9

c-HBP, circular-hepatobiliary-phase; p-HBP, pseudo-random-hepatobiliary-phase.

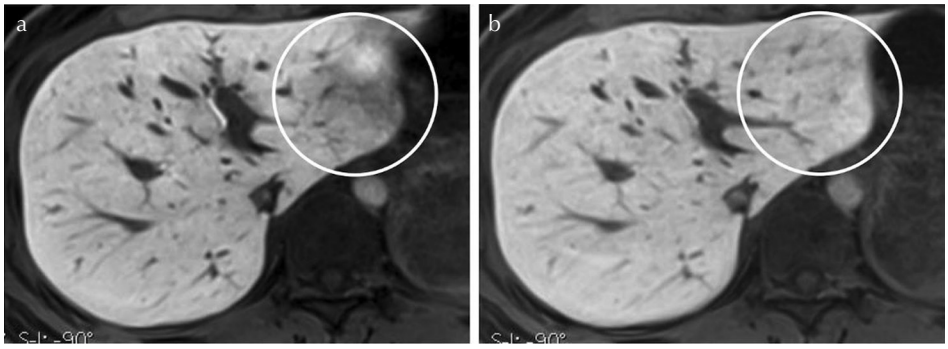

Fig. 5 Hepatobiliary-phase images obtained with circular- (**a**) and pseudo-random trajectory scanning (**b**) in a 39-year-old woman. Motion artifacts in the left lobe (circles) are suppressed on the image (**b**). The visibility of intrahepatic vessels is slightly better on the image (**a**).

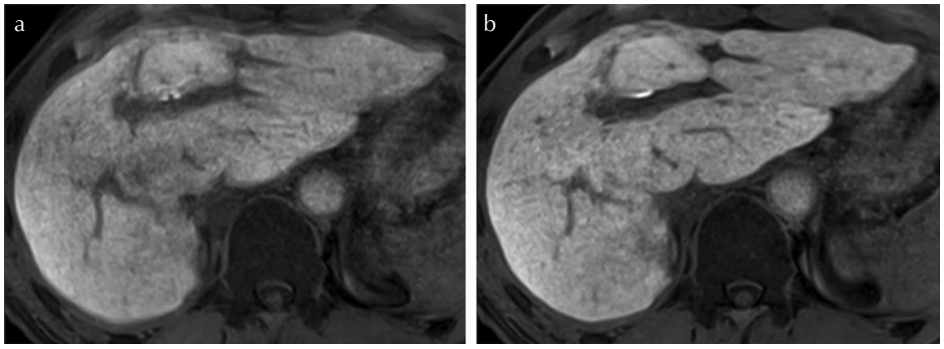

Fig. 6 Hepatobiliary-phase images obtained with circular- (**a**) and pseudo-random trajectory scanning (**b**) in a 55-year-old man. The image quality of (**b**) is better than of (**a**) and the sharpness of the liver edge and the visibility of intrahepatic vessels is also better on (**b**).

the sharpness of the liver edge (mean 4.0 vs 4.0 for p-HBP and c-HBP, $P = 0.57$) nor the score assigned for the visibility of intrahepatic vessels (mean 3.7 vs 3.6 for p-HBP and c-HBP, $P = 0.11$) (Table 2 and Fig. 6). Table 3 shows that the overall image quality of p-HBP was superior to c-HBP (mean 3.6 vs 3.3 for p-HBP and c-HBP, $P < 0.01$). Interobserver agreement was rated as good (κ-value range 0.78–0.84).

Table 2 Subjective image quality scores for sharpness of the liver edge and visibility of intrahepatic vessels

	Liver edge		Vessel	
	c-HBP	p-HBP	c-HBP	p-HBP
Score 1	0	0	0	0
Score 2	1	2	8	5
Score 3	16	10	22	19
Score 4	30	37	20	26
Score 5	15	13	12	12

Data are number of patients. c-HBP, circular-hepatobiliary-phase; p-HBP, pseudo-random-hepatobiliary-phase.

Table 3 Subjective overall image quality scores

	c-HBP	p-HBP
Score 1	0	0
Score 2	7	6
Score 3	29	21
Score 4	22	25
Score 5	4	10

Data are number of patients. c-HBP, circular-hepatobiliary-phase; p-HBP, pseudo-random-hepatobiliary-phase.

Discussion

In our computer simulation study, visible motion artifacts and image noise were lower on pseudo-random than circular images. Our phantom study yielded similar findings. The results of our clinical study also showed that with respect to motion artifacts, p-HBP images received significantly better scores and the overall image quality score was higher for p-HBP than c-HBP scans. Thus, we concluded that as the motion artifact was reduced using pseudo-random trajectory scanning, it yielded better image quality than circular trajectory scanning.

As pseudo-random acquisition suppresses artifacts by dispersing them into the background,[9] they may be increased in some areas especially in slice and phase direction. Indeed, on our computer-simulated pseudo-random images but not on circular images we observed a slight artifact on the anterior side of the liver, indicating that this slight artifact may obscure the focal hepatic lesion. Also, artifact dispersion into the background of pseudo-random images may degrade anatomic detail such as lesion edges and small structures. In 8 out of 62 patients (13%), the score assigned for visibility of intrahepatic vessels was lower on p-HBP than c-HBP images although the difference was not significant. Based on our findings we suggest that in patients undergoing hepatic MRI studies, p-HBP complements c-HBP scanning.

On abdominal MRI scans, respiratory motion artifacts are suppressed more easily than motion artifacts due to intestinal peristalsis. The navigator-gating technique is used to

identify motion-corrupted measurements and to acquire the measurements again when the target returns close to its anatomic baseline position.[15] Consequently, the navigator-gating technique is effective for suppressing respiratory but not motion artifacts due to intestinal peristalsis because the bowel does not periodically return to a fixed position. The administration of butylscoplamin, an antiperistaltic agent, has been reported to reduce peristaltic artifacts on abdominal MRI scans.[8] However, butylscoplamin may induce the adverse effects such as dry mouth, dizziness, blurred vision, nausea, headache, drowsiness, tachycardia, and weakness. Also, its routine administration to patients undergoing abdominal MRI decreases throughput and increases costs. Therefore, we suggest p-HBP scanning as a useful technique for suppressing peristaltic artifacts.

High spatial resolution images helps to improve the detection of small lesions and the characterization of lesions in terms of better delineation of morphological features, indicating that resolution of p-HBP should be higher. For p-HBP with higher resolution the number of shots or segments should be changed. However, in our scanning protocol chemical-shift selective sequence pulse is applied immediately before each shot, meaning that increment of the number of segments may lead the insufficient fat suppression on images. Thus, p-HBP with higher resolution may be acquired with increment of the number of shots. Further study is needed on this point.

Our study has some limitations. The study population was relatively small and our investigation was retrospective and performed at a single institution. Therefore, we offer our findings as preliminary. We performed only qualitative evaluation in our clinical study. Our use of the parallel-imaging acquisition technique rendered quantitative analysis of the signal intensity on images acquired with the different techniques difficult. However, our simulation and phantom study showed that the image noise was lower on pseudo-random than circular images. Next, we did not evaluate focal hepatic lesions. Studies are needed to determine whether the diagnostic performance of p-HBP is superior to c-HBP imaging for the evaluation of focal hepatic lesions. In addition, as stated above, pseudo-random acquisition suppresses artifacts by dispersing them into the background, resulting in the change of signal intensity of some area due to the dispersed artifact. Signal intensity at p-HBP should be considered not to be same to that at c-HBP. Finally, pseudo-random trajectory can be applied to breath-hold sequence, meaning that this trajectory may be used for arterial phase imaging, essential phase for evaluation of hepatic lesions.[16,17] Further investigation for utility of pseudo-random trajectory on arterial phase scanning is needed.

Conclusion

On gadoxetic acid-enhanced HBP scans, p-HBP scanning suppressed motion artifacts due to intestinal peristalsis and yielded better image quality than c-HBP scanning.

Conflicts of Interest

Kazuo Awai received a research grant from Hitachi, Ltd; Takashi Nishihara, Kuniaki Harada, Masahiro Takizawa, and Yoshitaka Bito are employees of Hitachi, Ltd.; the other authors declare that they have no conflicts of interest.

References

1. Sano K, Ichikawa T, Motosugi U, et al. Imaging study of early hepatocellular carcinoma: usefulness of gadoxetic acid-enhanced MR imaging. Radiology 2011; 261:834–844.
2. Guo J, Seo Y, Ren S, et al. Diagnostic performance of contrast-enhanced multidetector computed tomography and gadoxetic acid disodium-enhanced magnetic resonance imaging in detecting hepatocellular carcinoma: direct comparison and a meta-analysis. Abdom Radiol (NY) 2016; 41:1960–1972.
3. Ye F, Liu J, Ouyang H. Gadolinium ethoxybenzyl diethylenetriamine pentaacetic acid (Gd-EOB-DTPA)-enhanced magnetic resonance imaging and multidetector-row computed tomography for the diagnosis of hepatocellular carcinoma: a systematic review and meta-analysis. Medicine (Baltimore) 2015; 94:e1157.
4. Muhi A, Ichikawa T, Motosugi U, et al. Diagnosis of colorectal hepatic metastases: comparison of contrast-enhanced CT, contrast-enhanced US, superparamagnetic iron oxide-enhanced MRI, and gadoxetic acid-enhanced MRI. J Magn Reson Imaging 2011; 34:326–335.
5. Inoue Y, Hata H, Nakajima A, Iwadate Y, Ogasawara G, Matsunaga K. Optimal techniques for magnetic resonance imaging of the liver using a respiratory navigator-gated three-dimensional spoiled gradient-recalled echo sequence. Magn Reson Imaging 2014; 32:975–980.
6. Lee ES, Lee JM, Yu MH, et al. High spatial resolution, respiratory-gated, T_1-weighted magnetic resonance imaging of the liver and the biliary tract during the hepatobiliary phase of gadoxetic acid-enhanced magnetic resonance imaging. J Comput Assist Tomogr 2014; 38:360–366.
7. Yoon JH, Lee JM, Lee ES, et al. Navigated three-dimensional T_1-weighted gradient-echo sequence for gadoxetic acid liver magnetic resonance imaging in patients with limited breath-holding capacity. Abdom Imaging 2015; 40:278–288.
8. Dosdá R, Martí-Bonmatí L, Ronchera-Oms CL, Mollá E, Arana E. Effect of subcutaneous butylscopolamine administration in the reduction of peristaltic artifacts in 1.5-T MR fast abdominal examinations. Eur Radiol 2003; 13:294–298.
9. Lin C, Bernstein MA. 3D magnetization prepared elliptical centric fast gradient echo imaging. Magn Reson Med 2008; 59:434–439.
10. Winkelmann S, Schaeffter T, Koehler T, Eggers H, Doessel O. An optimal radial profile order based on the golden ratio for time-resolved MRI. IEEE Trans Med Imaging 2007; 26:68–76.
11. Phelps AS, Naeger DM, Courtier JL, et al. Pairwise comparison versus Likert scale for biomedical image assessment. AJR Am J Roentgenol 2015; 204:8–14.
12. Likert R. A technique for the measurement of attitudes. Arch Psychol 1932; 140:5–55.

13. Kajita K, Goshima S, Noda Y, et al. Thin-slice free-breathing pseudo-golden-angle radial stack-of-stars with gating and tracking T_1-weighted acquisition: an efficient gadoxetic acid-enhanced hepatobiliary-phase imaging alternative for patients with unstable breath holding. Magn Reson Med Sci 2019; 18:4–11.
14. Svanholm H, Starklint H, Gundersen HJ, Fabricius J, Barlebo H, Olsen S. Reproducibility of histomorphologic diagnoses with special reference to the kappa statistic. APMIS 1989; 97:689–698.
15. Ehman RL, Felmlee JP. Adaptive technique for high-definition MR imaging of moving structures. Radiology 1989; 173:255–263.
16. Bruix J, Sherman M. Management of hepatocellular carcinoma: an update. Hepatology. 2011; 53:1020–1022.
17. Motosugi U, Ichikawa T, Araki T. Rules, roles, and room for discussion in gadoxetic acid-enhanced magnetic resonance liver imaging: current knowledge and future challenges. Magn Reson Med Sci 2013; 12:161–175.